THE JOURNAL OF PHYSICAL CHEMISTRY C

Article

pubs.acs.org/JPCC

Bimetallic Borohydrides in the System $M(BH_4)_2$–KBH_4 (M = Mg, Mn): On the Structural Diversity

Pascal Schouwink,*[,†] Vincenza D'Anna,[‡] Morten Brix Ley,[§] Latévi Max Lawson Daku,[‡] Bo Richter,[§] Torben R. Jensen,[§] Hans Hagemann,[‡] and Radovan Černý*[,†]

[†]Laboratory of Crystallography, Department of Condensed Matter Physics, and [‡]Department of Physical Chemistry, University of Geneva, 1211 Geneva, Switzerland

[§]Center for Materials Crystallography (CMC), Interdisciplinary Nanoscience Center (iNANO), and Department of Chemistry, Aarhus University, Langelandsgade 140, DK-8000 Århus C, Denmark

Supporting Information

ABSTRACT: Four novel bimetallic borohydrides have been discovered, $K_2M(BH_4)_4$ (M = Mg or Mn), $K_3Mg(BH_4)_5$, and $KMn(BH_4)_3$, and are carefully investigated structurally as well as regarding their decomposition reaction mechanism by means of in situ synchrotron radiation powder X-ray diffraction (SR-PXD), vibrational spectroscopies (Raman and IR), thermal analysis (TGA and DTA), and ab initio density functional theory (DFT) calculations. Mechano-chemical synthesis (ball-milling) using the reactants KBH_4, α-$Mg(BH_4)_2$, and α-$Mn(BH_4)_2$ ensures chlorine-free reaction products. A detailed structural analysis reveals significant similarities as well as surprising differences among the two isomorphs $K_2M(BH_4)_4$, most importantly concerning the extent to which the complex anion $[M(BH_4)_4]^{2-}$ is isolated in the structure. Anisotropic thermal expansion and an increase in symmetry at high temperatures in $K_3Mg(BH_4)_5$ is ascribed to the motion of BH_4 groups inducing hydrogen repulsive effects, and the dynamics of $K_3Mg(BH_4)_5$ are investigated. Decomposition in the manganese system proceeds via the formation of $KMn(BH_4)_3$, the first perovkite type borohydride reported to date.

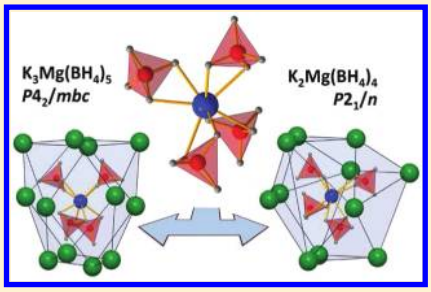

INTRODUCTION

The continuously growing family of potential hydrogen storage materials for mobile applications includes metal borohydrides among the most promising candidates due to their high gravimetric hydrogen densities and somewhat tunable decomposition temperatures.[1−3] Recently, the latter point has been in focus, in terms of double-cation compounds containing the BH_4-group. Empirical relationships between Pauling electronegativities and decomposition temperatures have been suggested previously.[4,5] The more challenging attempt to find systematic structure−property relationships is somewhat hampered by insufficient structural insight, which has prompted the current investigation. Moreover, the stability of compounds as well as their decomposition mechanisms remain not fully understood, regarding the release of hydrogen or diborane as well as the formation of higher boranes, metal hydrides, or borides, on one hand, and the mechanism of decomposition itself, on the other. This may include genuine decomposition, melting without gas release, or dissociation to starting materials. Many of these less favorable effects can be manipulated in a targeted manner, for example, by alteration of grain size[6−8] or using selected additives.[8]

Metal borohydrides exhibit a great structural variety such as in ionic and covalent bonding including the intriguing coordination of hydrogens to cations as well as potential disorder. These compounds therefore receive significant attention from a fundamental science point of view. Anion substitution was first discovered in the $LiBH_4$–$LiCl$ system,[9,10] which later led to the discovery of fast lithium ion conductivity.[11] Recently, a solid cation solution was discovered in $Mg_xMn_{1-x}(BH_4)_2$, nearly over the whole compositional range.[12] Solubility has a slight effect on the decomposition temperature as the latter is controlled by the more electronegative metal, but may alter gravimetric hydrogen density considerably.

The present investigation aims at extending the results from the binary Mg−BH_4 and Mn−BH_4 systems to the ternary K−M−BH_4, M = Mg or Mn, systems, providing insight into the structural behavior of tetrahedrally coordinated magnesium and manganese while crossing the boundary between framework and ionic solids. It focuses on the structural and geometric variations arising due to cation substitution on the central site of the main building block $[M(BH_4)_4]^{2-}$, occurring in three out of four new reported compounds, $K_2M(BH_4)_4$ (M = Mg or Mn), $K_3Mg(BH_4)_5$, and $KMn(BH_4)_3$. A thorough structural analysis is undertaken, comparing the results to those obtained in other studies of related systems K−M−BH_4 (M = Zn or Cd).[13,14] The four new compounds are synthesized mechano-chemically and studied by in situ synchrotron radiation powder X-ray diffraction (SR-PXD), vibrational spectroscopy (Raman

Received: December 21, 2011
Revised: March 16, 2012

   dx.doi.org/10.1021/jp212318s | J. Phys. Chem. C XXXX, XXX, XXX–XXX

and IR), thermal analysis (TGA and DTA), as well as ab initio calculations performed within density functional theory (DFT).[15,16]

EXPERIMENTAL SECTION

Sample Preparation. All samples were prepared mechanochemically by ball-milling with a Fritsch Pulverisette 7 high-energy planetary ball-mill. The starting materials for each sample (~1.5 g in total) were preground in an agathe mortar. The K−Mg−BH_4 samples were ball-milled at 600 rpm, for a total time of 350 min, using a 25 mL stainless steel grinding bowl sealed with a lid and a Viton O-ring. Three stainless steel balls of 15, 12, and 10 mm diameter were used as milling medium, resulting in a powder to ball mass ratio of ca. 1:16. Milling was interrupted every 10 min to allow for cooling of the milling vessel for 5 min. Because of the smaller amount of $Mn(BH_4)_2$ available for synthesis, the milling parameters had to be adjusted so as to provide similar conditions. The synthesis of $Mn(BH_4)_2$ is still not fully under control, and all but one synthesis resulted in an excess of LiCl; thus these products could not be used for a chlorine-free synthesis. In addition, the use of Me2S as extractant solvent prompted us to use minimal quantities of materials. The reason for this is that Me2S is extremely unpleasant in its odor, and it is virtually impossible to avoid having some leaks due to its high volatility. A total mass of 0.5 g was used here, milled at 600 rpm for 120 min with a cooling break of 2 min every 2 min (the powder to ball mass ratio was approximately 1:49). A complete list of samples and milling conditions is provided in Table 1.

Table 1. Composition of Sample Mixtures and Resulting Products of Ball-Milling

sample name	reactants	molar ratios	ball-milling products
A_Mn1	KBH_4−$MnCl_2$	4:3	$K_2Mn(BH_4)_4$, $KMnCl_3$
B_Mg1	KBH_4−$Mg(BH_4)_2$	1:1	$K_2Mg(BH_4)_4$, $Mg(BH_4)_2$
B_Mg2	KBH_4−$Mg(BH_4)_2$	2:1	$K_3Mg(BH_4)_5$, $K_2Mg(BH_4)_4$, KBH_4
B_Mn1	KBH_4−$Mn(BH_4)_2$	1:1	$K_2Mn(BH_4)_4$, $Mn(BH_4)_2$
B_Mn2	KBH_4−$Mn(BH_4)_2$	2:1	$K_2Mn(BH_4)_4$, KBH_4

Manganese borohydride, $Mn(BH_4)_2$, was prepared using 2.50 g (20.0 mmol, 1 equiv) of $MnCl_2$ (Sigma-Aldrich, anh., 99.99%) suspended in ether at room temperature followed by addition of 0.70 g (32.0 mmol, 1.6 equiv) of $LiBH_4$ (Sigma-Aldrich ≥95%). After being stirred at room temperature for 30 min, a pale yellow suspension formed; upon further stirring, the yellow substance dissolved, and the reaction was allowed to proceed overnight. The mixture was filtered using a microporous glass Büchner filter. The filtrate was collected and concentrated in vacuo, yielding a pale yellow solid. The solid material was further dried on a vacuum line (4×10^{-2} mbar), initially at room temperature, and then at 110 °C for 12−16 h. The material obtained was a pale yellow powder (1.3 g, yield 70%), consisting of $Mn(BH_4)_2$. The synthesis of the reactant magnesium borohydride, $Mg(BH_4)_2$, is described elsewhere.[17] Potassium borohydride, KBH_4, was used as received from Fluka (95% purity). All sample handling was done under argon atmosphere in a glovebox with a circulation purifier $p(O_2, H_2O)$ < 0.1 ppm.

Thermal Analysis. Simultaneous thermogravimetric analysis (TG) and differential thermal analysis (DTA) were performed on samples 2:1 and 1:1 of the K−Mg−BH_4 system using a Netzsch STA449C Jupiter instrument in the temperature range from room temperature to 773 K, at a heating rate $\Delta T/\Delta t$ = 10 °C/min using corundum crucibles with lids as sample holders packed in a glovebox. The experiments were conducted in a helium (4.6) atmosphere. Because of the small amount of sample, thermal analysis was only performed on the K−Mg system.

In Situ Synchrotron Radiation Powder X-ray Diffraction. Diffraction data were collected on the Swiss Norwegian Beamlines BM01A and BM01B (ESRF, Grenoble, France). Selected wavelengths were 0.72846(2), 0.69671(2), and 0.69776(1) Å, respectively, for three different beamtimes on BM01A. The sample to detector distance was set to 250 mm for temperature ramps (room temperature to 500 K, rate 1 or 2 K/min), and to 400 mm for single scans used for indexing. Temperature was controlled with the Oxford Cryostream 700+. The setup was calibrated with LaB_6 prior to experiment. Powder samples were loaded into capillaries of 0.7 mm diameter, which were rotated by 1°/s during data collection, at an exposure time of 30 s. Intensities were registered on a MAR 345 image plate detector, the 2D-powder data were then integrated with the FIT2D software,[18] and standard deviations were added applying Poisson statistics according to the detector geometry.[19] The data set that served for indexing and structure solution of the Mn-compound was collected on the High Resolution Beamline BM01B with a multicrystal analyzer, at a wavelength of 0.50120(3) Å.

Structure Solution and Refinement. All structures presented here were indexed and subsequently determined in direct space modeling with Global Optimization methods implemented in the program FOX.[20] The crystallographic information files (CIF) are given in the Supporting Information. The structure of the first new compound $K_2M(BH_4)_4$ (M = Mn, Mg) was solved from the data set collected on sample A_Mn1, which is not shown as all structural features are identical to the chlorine-free synthesis. All attempts to index the unit cell from image plate data failed initially due to the severe peak overlap and the temperature-dependent interplay of two polymorphs of the ternary Chloride $KMnCl_3$, crystallizing in structure types $GdFeO_3$[21] and NH_4CdCl_3, respectively.[22] Thus, high resolution data were acquired, which, in conjunction with careful inspection of T-ramps, allowed for indexing in a monoclinic cell with a = 8.1392(5), b = 9.8471(6), c = 12.7471(8) Å, β = 100.530(6)°, V = 1004.44(11) Å^3 (final values from Rietveld refinement at 293 K) on the basis of 11 Bragg peaks. Furthermore, syntheses were repeated later on using pure binary borohydrides to avoid chlorine impurities. All of the compounds here are thus products of a chlorine-free synthesis. During search in direct space, BH_4 groups were treated as rigid bodies with one common B−H distance of 1.14 Å. $K_2Mn(BH_4)_4$ was solved in space group $P2_1/n$, which is a maximal nonisomorphic subgroup of $Pnma$, this being the space group of the room temperature K_2SO_4 prototype.[23] $K_2Mg(BH_4)_4$, isomorphic to the K−Mn compound, required no structure solution as the model is isostructural with a = 8.1791(9) Å, b = 9.8842(7) Å, c = 12.7492(10) Å, β = 100.74(3)(6)°, V = 1012.66(15) Å^3 (final values from Rietveld refinement at 293 K). The agreement factors for all refinements on all of the studied samples are given in Table 2.

dx.doi.org/10.1021/jp212318s | J. Phys. Chem. C XXXX, XXX, XXX−XXX

Table 2. Lattice Parameters and Agreement Factors Extracted from Rietveld Refinement with TOPAS as well as DFT Calculation for the Variable Cell Case[a]

compound	a (Å)	b (Å)	c (Å)	β (deg)	V (Å^3)	SG	R_{Bragg}, R_{wp}, (%), χ^2
$K_2Mn(BH_4)_4$	8.1392(5)	9.8471(6)	12.7471(8)	100.530(6)	1004.44(11)	$P2_1/n$	1.67, 5.10, 4.08
$K_2Mn(BH_4)_4$	8.1375(7)	9.8456(7)	12.7420(12)	100.552(6)	1003.61(15)	$P2_1/n$	0.64, 5.29, 4.4 × 10^3
$K_2Mg(BH_4)_4$	8.1791(9)	9.8842(7)	12.7492(10)	100.74(3)	1012.66(15)	$P2_1/n$	0.81, 4.91, 3.0 × 10^3
variable cell	7.978	9.535	13.348	93.276	1013.76		
$K_3Mg(BH_4)_5$	8.9706(5)	8.9706(5)	15.9486(11)		1283.42(15)	$P4_2bc$	1.49, 5.77, 6.4 × 10^3
$K_3Mg(BH_4)_5$	8.9693(6)	8.9693(6)	15.9501(13)		1283.15(19)	$P4_2/mbc$	2.19, 7.51, 1.1 × 10^4

[a]Two models related by inversion centering were tested for the case of $K_3Mg(BH_4)_5$. The very low value of χ^2 for sample A_Mn1 (first row, from chloride synthesis, see Table 1) may be explained by the lower counting rate of the analyzer crystal. R_{wp} is not corrected for background.

DFT calculations were performed to determine the energetically most favorable orientation of BH_4 groups, and the suggested structural model from FOX was refined in TOPAS,[24] treating BH_4 as a translational group with three degrees of freedom and at the same time allowing for an additional three degrees of freedom to treat the orientation of the tetrahedron as correctly as possible. To constrain the movement of BH_4 groups during refinement, we introduced four antibumps for $K_2M(BH_4)_4$: M−H = 1.8, M−B = 2.2, K−H = 1.8, and B−B = 3.0 Å. The orientations of BH_4 groups found by Rietveld refinements in TOPAS compare well to those suggested by DFT. All structural models presented here are thus results of refinements in TOPAS on samples containing no chlorine. During refinement, $[BH_4]^-$ anions were treated as semirigid ideal tetrahedral groups with one common refined B−H distance. The refined structural models were checked for higher symmetry in the ADDSYM program of PLATON.[25] The cell parameters as well as the final agreement factors are given in Table 2 for all compounds. $K_3Mg(BH_4)_5$ was initially indexed from laboratory PXD data measured at room temperature, as the sample quality was sufficiently high for the chloride-free syntheses. The metric of the unit cell was found to resemble that of the prototype Cs_3CoCl_5.[26] However, inspection of systematic extinctions revealed a necessary loss of body centering to allow for weak Bragg signals, which are unambiguously assigned to the new compound. Thus, extinctions suggested a variety of subgroups of $I4/mcm$ (the prototype) equally sensible. Given this, the maximal subgroup $P4_2/nbc$ was assumed to be correct initially. However, a detailed analysis using Rietveld refinements finally pointed toward $P4_2bc$, a second-order subgroup to the prototype $I4/mcm$, to generate the most accurate fit to experimental data. PLATON was run to check for missed symmetry, and inversion symmetry was suggested, which was subsequently tested by Rietveld refinement. The resulting space group $P4_2/mbc$ is a maximal subgroup of $I4/mcm$ and was adopted for all refinements in the following, for reasons outlined below. Refinements were carried out in TOPAS using the same procedure as stated above and stabilizing with the help of antibumps Mg−H = 1.8, Mg−B = 2.2, K−H = 1.8, H−H = 2.1, and B−B = 3.0 Å.

Thermal evolution of lattice parameters was studied by sequential refinement, and atomic positions were fixed to room temperature values as well as the zero-shift.

Raman and Infrared Spectroscopy. Raman spectra were collected on samples B_Mg1 and B_Mn1 on a homemade setup using a green laser (λ = 514.5 nm) and a Sciencetech 9040 monochromator. Powders were placed on a XRD sample holder and sealed airtight with a foil, and the laser was focused with an objective 50×. Laser power was constrained to small values of about 1−2 mW to avoid sample damage. The spectral resolution obtained with a grating of 600 lines/mm is about 4−5 cm^{-1}. Signals were registered on a liquid nitrogen cooled Spec-10 CCD camera working at 153 K.

Infrared spectra were obtained on samples B_Mg1 and B_Mg2 of the K−Mg system; unfortunately, the very small amount of sample prevented us from a comparison with the Mn system. A Biorad Excalibur instrument equipped with a Specac low temperature Golden Gate Diamond ATR system was used, and the spectral resolution was about 1 cm^{-1}.

Computational Details. Periodic DFT calculations were employed with the aim of supporting the structural model found for $K_2Mg(BH_4)_4$. The calculations were performed within the generalized gradient approximation (GGA)[27] with the ABINIT package (Version 6.2.2), which is based on pseudopotentials and planewaves.[28] Troullier−Martin pseudopotentials were used in the separable Kleinman−Bylander form.[29,30] In the $P2_1/n$ setting considered for the description of the crystal structure of $K_2Mg(BH_4)_4$, we employed a 2 × 2 × 1 k-point Monkhorst−Pack grid[31] and expanded the wave functions in planewaves up to a kinetic-energy cutoff of 80 hartree.

Molecular DFT calculations were also carried out on the isolated cluster $[Mg(BH_4)_4]^{2-}$ with the B3LYP functional[32−36] and the TZVP basis set of triple-ζ polarized quality,[37] using the Turbomole package.[38] They consisted of the optimization of the structure of the cluster followed by a frequency analysis, whose results confirmed that the located extremum is a true minimum.

RESULTS AND DISCUSSION

Synthesis and Initial Phase Analysis. One of the aims of this study was to elucidate the similarities in crystal chemistry between bimetallic compounds bearing the tetrahedral complex anion $[M(BH_4)_4]^{2-}$ (M = Mg, Mn), to extend the analogies from binary[12] to ternary manganese and magnesium-containing borohydrides. A chlorine-free synthesis starting from pure binary compounds provides the prerequisites for such a comparison. As Li- and Na-containing syntheses do not provide ternary compounds, KBH_4 was the reactant of choice to successfully obtain the bimetallic phases.

The reaction schemes as confirmed by Rietveld refinement for the samples discussed here are the following. Formulas correspond to genuine reactions taking place as deduced from refinement, and thus reaction stoichiometries differ from the "real" ratios of synthesized mixtures. Hence, unreacted quantities and impurities are disregarded in the formula. Composition 1:1 results in a very similar reaction for both systems (M = Mg or Mn):

$$4KBH_4 + 2M(BH_4)_2 \rightarrow 2K_2M(BH_4)_4 \quad (1)$$

dx.doi.org/10.1021/jp212318s | J. Phys. Chem. C XXXX, XXX, XXX−XXX

Unreacted binaries $M(BH_4)_2$ are observed for ratios 1:1 in both cases M = Mg, Mn. However, an ideal ratio of KBH_4:$M(BH_4)_2$ = 2:1 does not yield a single phase product $K_2M(BH_4)_4$ by completing the reaction, but results in the formation of an additional new phase in the Mg system:

$$5KBH_4 + 2Mg(BH_4)_2 \rightarrow K_2Mg(BH_4)_4 + K_3Mg(BH_4)_5 \quad (2)$$

MgH_2 as well as Mg were observed as impurities, however not originating, as assumed originally, from a mechanochemically induced decomposition of the binary, but from the wet chemistry synthesis. In the manganese system, no additional new phase forms; thus merely an excess of KBH_4 is observed for the 2:1 mixture. Synthesis products as well as their stabilities are subject to ball-milling conditions and complicated phase equilibriums. Therefore, the ideal 2:1 ratio of precursors does not yield a single phase product of $K_2M(BH_4)_4$, similar to $LiK(BH_4)_2$ in the KBH_4–$LiBH_4$ system.[39] Furthermore, the milling conditions had to be altered slightly for the manganese syntheses (see above) due to the very low quantity of sample available, which probably resulted in somewhat "softer" milling. Judging from the decomposition mechanism of $K_3Mg(BH_4)_5$ (see below), it appears likely that this phase should form from $K_2M(BH_4)_4$ interacting with residual KBH_4, depending on external variables. Thus, even though no new compound of stoichiometry 3:1:5 was found in the manganese system, its existence shall not be excluded. Evidence for the just stated is found in the different degrees of crystallinity between powder samples of both systems, manganese and magnesium. Peaks are broader in the latter, indicating the possibility of overmilling. On one hand, manganese may intrinsically form better crystallized compounds as it is known for the K–Zn–BH_4 system;[13] on the other hand, the presence of Mg and MgH_2 in room temperature data already points toward overmilling, as they are probably generated by going beyond the stability of $Mg(BH_4)_2$.

In sample B_Mn2, there is remnant amorphous $Mn(BH_4)_2$, which in turn is an indicator of the compound possibly being on the verge of stability before decomposing. If, on the other hand, we assume that a longer milling time may result in the formation of $K_3M(BH_4)_5$, we could expect the following. After a sufficient amount of $K_2M(BH_4)_4$ is formed, and provided that the milling energy, meaning temperature as well as pressure inside the milling vessel, is high enough, residual KBH_4 (still present in all 2:1 samples after milling) could infiltrate the structure of $K_2M(BH_4)_4$. This, according to the results shown below, would lead to an intergrown network generated at high energies, maybe also to disordering phenomena. Stopping ball-milling results in quenching of this intergrowth structure, which consecutively may be considered metastable at room conditions due to internal structural properties. Raising the temperature, and in the absence of the pressure generated during milling, will then result in annealing and shifting the equilibrium toward the stable phase, which in this case is $K_2M(BH_4)_4$. Thus, the reverse reaction will be taking place, resulting in segregation of the intergrowth. This is in fact what we observe for the K–Mg–BH_4 system. To verify these assumptions, it should be useful to scan the P–T diagram of composition 2:1. Thus, $K_3Mn(BH_4)_5$ may exist in a narrow P–T window in the phase diagram, which will be the subject of a future research project.

Crystal Structure of $K_2M(BH_4)_4$. The refined lattice parameters of both isomorphs are shown in Table 2, and the Rietveld plots are shown in the Supporting Information (Figures S1 and S2). The crystal structure of $K_2M(BH_4)_4$ is a monoclinically distorted derivative of β-K_2SO_4, with M on the S position and BH_4 groups on the O positions, all occupying general position *4e*. Similar observations are made for new compounds found in the systems K–M–BH_4 (M = Zn or Cd).[13,14] The most prominent building block is the complex tetrahedral anion $[M(BH_4)_4]^{2-}$ with bidentate M···H_2B bonding scheme shown in Figure 1 for M = Mg, as calculated

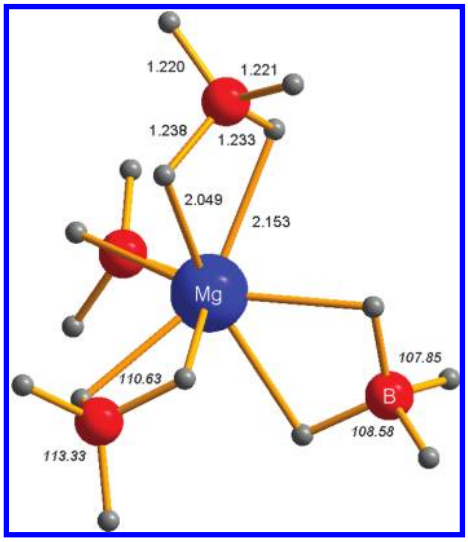

Figure 1. The tetrahedral complex anion $[M(BH_4)_4]^{2-}$, shown for $[Mg(BH_4)_4]^{2-}$ as calculated by DFT. The interatomic distances [Å] are shown in regular letters, while bond angles [deg] are in italics.

by DFT. The inner B–H distances are longer than the outer ones, while the inner H–B–H angle of the Mg–H_2B fragment is smaller than that of the opposing K–H_2B fragment, yet with both being larger than the angles of the noncoordinating H_2B edges (see Figure 1). This agrees well with the DFT results obtained for the triangular complex $[Zn(BH_4)_3]^-$.[13] Even though the isolated calculated molecule is less distorted than the refined one, the mean Mg–B distances change very little (2.5379 Å) for DFT versus 2.5027(1) Å for XRD). The same holds for a comparison with the periodic calculation in $K_2Mg(BH_4)_4$, where the average Mg–B distance is 2.4294 Å (see Table 3). Molecular calculations have already been reported for the isolated complex anion $[Mn(BH_4)_4]^{2-}$,[40] but the obtained mean Mn–B distances agree poorly with experimentally determined bond lengths in $K_2Mn(BH_4)_4$, that

Table 3. Comparison of the Local Environment of the Complex Tetrahedral Anion $[M(BH_4)_4]^{2-}$ with M = Mg, Mn, Zn, Cd[a]

compound	average M–B	B–K/M–B	$V(MK_{11})/V(MB_4)$
$K_2Mn(BH_4)_4$	2.4544(51)	1.41	36.61
$K_2Mg(BH_4)_4$	2.5027(31)	1.38	34.33
fixed cell	2.4402	1.39	35.29
variable cell	2.4294	1.35	36.81
$K_2Zn(BH_4)_4$	2.466(17)	1.33	31.85
$K_2Cd(BH_4)_4$	2.881(10)	1.11	24.02
$KSc(BH_4)_4$	2.3204(3)	1.64	31.56
$K_3Mg(BH_4)_5$	2.4369(77)	1.45	38.23 $V(MK_{12})/V(MB_4)$

[a]DFT results are denoted fixed and variable cell, respectively, as stated in the text. $KSc(BH_4)_4$ is listed for comparison.

dx.doi.org/10.1021/jp212318s | J. Phys. Chem. C XXXX, XXX, XXX–XXX

is, Mn−B distances of 2.17 (DFT[40]) and 2.4544(51) Å (this work). Given the good agreement found for the molecular optimization on the isolated $[Mg(BH_4)_4]^{2-}$ anion, we assume that this discrepancy may be owed to the inherent difficulties when performing DFT on transition metals. Therefore, we did not attempt any new theoretical work on the K−Mn−BH_4 system in this study. The environment of $[M(BH_4)_4]^{2-}$ described by its nearest neighbors is a pentacapped trigonal prism, formed by a trigonal prism (monoclinically distorted) with its 3-fold axis lying parallel to *c*, and a strongly distorted equatorial plane of 5 K atoms. The same coordination polyhedron is found for the same stoichiometry in the K−Zn−BH_4[13] and K−Cd−BH_4[14] systems, with different degrees of distortion. Even in $KSc(BH_4)_4$, different in stoichiometry, the feature of the trigonal prism is conserved as a side monocapped trigonal prism.[41] This allows for a detailed comparison of the compounds, especially as the extent of isolation inside the *n*-capped prism serves as a measure for the degree of isolation of the complex anion, and thus as an indicator for potential trends toward structural frameworks. Comparing these facts among the here reported compounds, the manganese and magnesium isomorphs, reveals a slight difference in isolation of the complex tetrahedron. This will be discussed in detail below.

Periodic DFT calculations were performed on the Mg phase to support the structural model of this compound as solved ab initio from experimental data. To this end, the crystal structure was optimized with the cell parameters either kept fixed to their experimental values or allowed to relax. The large unit cell makes such calculations computationally demanding. Still, a tight convergence criterion corresponding to a maximum force of 5.0×10^{-5} Ha/bohr was used. This criterion could actually only be met for the variable-cell optimization, which converged very slowly. The fixed-cell optimization also showed quite a slow progression, and it proved necessary to stop it when it became clear that no more significant decrease could be expected (1) for the energy, which stayed constant to within 0.1 mHa, and (2) for the maximum force, which started oscillating about the value of 10^{-4} Ha/bohr. The fixed-cell-optimized structure thus obtained corresponds to a maximum force of 1.5×10^{-4} Ha/bohr. The fixed-cell and variable-cell optimized structures are available in the Supporting Information. The optimized values of the cell parameters are summarized in Table 2 along with the experimental data. They are in reasonably good agreement with experiment.

The difficulties met in optimizing the structure of the Mg phase can be ascribed to the large number of degrees of freedom characterizing the system, due to the fact that each atom in the unit cell is occupying a general position *4e*. Additionally, it is probable that convergence could not be reached easily because the minimum sought after is very shallow, at least within the accuracy of the approximate GGA functional used. Thus, the energy difference between the fixed-cell and variable-cell-optimized structures amounts to less than 1 mHa (~220 cm^{-1}); that is, less than the so-called chemical accuracy of 350 cm^{-1} (1 kcal/mol). The theoretical description of the structures of borohydrides is a delicate issue, which is receiving much attention.[42]

In the present case, the issues preventing an easy optimization during calculations are most likely due to the DFT description of the interactions or, equivalently, the packing forces determining the orientation of the BH_4 groups. However, given the structural complexity of this Mg phase, the study of these interactions and of their description within DFT would require a whole separate study and, for this reason, will not be elaborated here.

Nevertheless, the calculated structures do maintain all important features of the model solved from diffraction data, the MgK_{11} cage around the complex anion and the predominant bidentate Mg···H_2B bonding scheme. Even the local surroundings of the K^+ ions as defined by the neighboring B atoms are described quite well. The greatest difference between the refined and calculated structures is found in the degree of distortion of $[Mg(BH_4)_4]^{2-}$. DFT indeed predicts a much more regular tetrahedron, with values of 96.70−112.93° (variable cell) for the B−Mg−B angle, while they are spread over a greater range between 101.190(4)° and 124.34(3)° in the model refined from XPD, which in turn is much closer to DFT when optimizing the fixed cell: 102.57−118.28°. These differences remain quite minor. We can therefore conclude that the model obtained from the XPD is verified by the DFT calculations.

Crystal Structure of $K_3Mg(BH_4)_5$. $K_3Mg(BH_4)_5$ crystallizes in a structure closely related to Cs_3CoCl_5, which crystallizes in space group *I*4/*mcm*. The Rietveld plot can be found in the Supporting Information Figure S3. The loss of body centering for $K_3Mg(BH_4)_5$ (see structure solution part) is probably caused by the nonspheric nature of $[BH_4]^-$ occupying the chlorine positions of the prototype Cs_3CoCl_5. Interestingly, the BH_4 group occurs in two different environments, forming similar complex anions $[Mg(BH_4)_4]^{2-}$ as observed in the structure of $K_2Mg(BH_4)_4$, on one hand, while the second boron position only coordinates to potassium. This $[BH_4]^-$ is octahedrally coordinated, strongly resembling the local environment of $[BH_4]^-$ in KBH_4.

Hence, the structure of $K_3Mg(BH_4)_5$ has an intriguing nature and may well be characterized as an intergrowth of KBH_4 and $K_2M(BH_4)_4$. The substructure of KBH_4 can be approximated as a distorted inverse ReO_3-type, forming a three-dimensional network of corner-sharing BH_4K_6 octahedra, which are elongated in direction [001]. The internal B−K distances of the octahedron depend largely on the model chosen for refinement. The polar space group $P4_2bc$, on one hand, results in an off center position for B in the octahedral cage, the polarity of the space group having a correlation between octahedra as a consequence and thus the same offset of the central atom in *c* direction for all octahedra. We consider this highly improbable. Refinements in space group $P4_2/mbc$, on the other hand, allow for disordering B2 as well as K2 along the *c*-axis leading to generate one-dimensional disordered KBH_4 channels along [001], which is much more likely, especially considering the low onset of decomposition as well as the intrinsic tendency of BH_4 groups to show some disorder in these kinds of compounds. This is the reason, alluded to earlier on, for adopting this space group. The interatomic K−B distance of KBH_4 is 3.3653(2) Å.[43] The increase in the polyhedral volume of BH_4K_6 in $K_3Mg(BH_4)_5$ amounts to 6% with regards to that of the same octahedron in KBH_4. In compliance with symmetry, at room temperature (site symmetry of average position of B2 is 2/*m*), we have three different distances K−B for BH_4K_6 and referring to averaged atom positions, the longest being found along the *c*-axis between the central atom B2 and apical atoms K2, 3.9876(3) Å. This large increase along *c*, being the main cause of the larger polyhedral volume, relative to KBH_4 clearly reflects the positional disorder along this direction as refined in the

dx.doi.org/10.1021/jp212318s | J. Phys. Chem. C XXXX, XXX, XXX−XXX

structural model $P4_2/mbc$. The B2−K1 distances in the (001) plane are 3.2856(10) and 3.3364(13) Å, respectively. The discrepancy between the two may well be a result of orientational ordering effects of $[BH_4]^-$ in the (001) plane, causing different degrees of repulsive H−K interaction, meaning that the disorder is mainly of a positional character in one dimension, along *c*, and that rotational will be of less significance. It should be pointed out, nevertheless, that reliable refinements including rotational degrees of freedom were not possible due to the quality of data, and the resulting BH_4 orientations are strongly biased by the used antibump restraints. The second component, building up the intergrowth of $K_3Mg(BH_4)_5$, is found in the framework of bicapped trigonal prisms of MgK_8, interconnected via common edges. This may be considered as a pre-established environment for the pentacapped trigonal prism MgK_{11} of $K_2Mg(BH_4)_4$.

The effect of temperature on the structural evolution of $K_3Mg(BH_4)_5$ is expected to enhance disorder on the mentioned positions. This is evidenced by the refinement at 367 K (Figure 2, Rietveld plot in Supporting Information Figure S4).

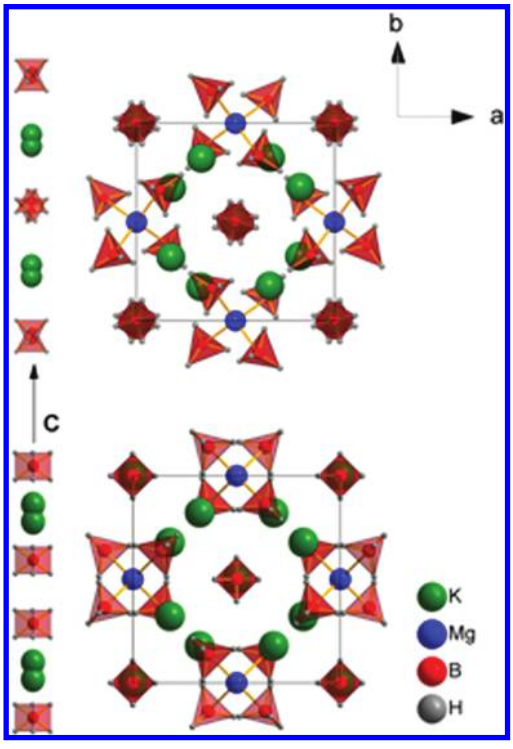

Figure 2. Comparison of the structure of $K_3Mg(BH_4)_5$ at room temperature (top) and 367 K (bottom). Internal reorientation of the complex anion $[Mg(BH_4)_4]^{2-}$ leads to a raise in symmetry $P4_2/mbc \rightarrow I4/mcm$. The increase in disorder is exemplified by the one-dimensional chain along *c* shown on the left.

However, not only does disorder increase, we also observe a gradual disappearance of extinctions fingerprinting the *P*-lattice during the first major decomposition event of $K_3Mg(BH_4)_5$ (Supporting Information Figure S8). This in turn implies a structural evolution toward a higher symmetry, i.e., $I4/mcm$ (Figure 2). As it is already present at room temperature, we can conclude that disorder is not the only thing driving this symmetry change. Disordering along *c* does not exclude body centering. We assume the geometry of the complex anion $[Mg(BH_4)_4]^{2-}$, with particular focus on the orientation of the BH_4 tetrahedrons, to be responsible for generating the *I* lattice, driven in turn by the dynamics of B2. This is also reflected in the thermal behavior of lattice parameters (Figure 3), which

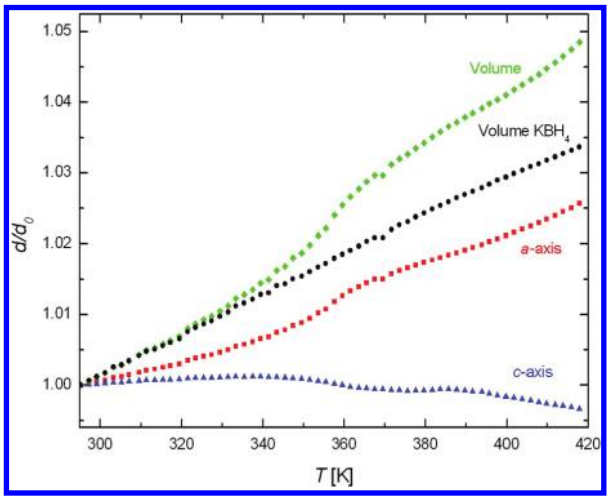

Figure 3. Evolution of normalized lattice parameters of $K_3Mg(BH_4)_5$ as a function of temperature. The refined volume of KBH_4 is shown as well to verify genuine changes in the new phase.

show nonlinearity over the corresponding temperature range where reflections disappear. To exclude systematic errors, the temperature evolution was cross-checked with the behavior of KBH_4, which remains linear. *R*-values also remain constant for all phases. As disorder is enhanced and $B2H_4^-$ starts to migrate along the *c* axis, it approaches $B1H_4$ ligands of the complex anion. At high degrees of disorder, all refined BH_4 groups are approximately lying in (001) planes. Hydrogen repulsion starts to play a significant role here, with H···H distances of 2.1315(1) Å approaching 2.1 Å, which is usually considered the lower limit for stable metal hydrides according to Switendick's criterion.[44] The B−Mg−B angle with its bisector along *c* shrinks from 96.64(3)° at room temperature to 95.02(4)° at 367 K, while the B−Mg−B angle with its bisector in the (001) plane increases slightly from 116.25(2)° to 117.15(2)°. Average bond lengths Mg−B of the complex anion decrease from 2.4369(77) (room temperature) to 2.4079(23) (367 K) Å, causing the volume of $[Mg(BH_4)_4]^{2-}$ to shrink by 4% while its host cage defined by K_{12} gains 4% in size ($V(MgK_{12})/V(MB_4)$ goes from 1.45 at room temperature to 1.49 at 367 K). The refined size-decrease of the central complex anion in MgK_{12} is illustrative of Coulomb interactions between different BH_4 groups, the disordered group $B2H_4$ closing in on $B1H_4$ (B1 pertaining to the complex anion) at higher temperatures and thus causing the negative thermal expansion of $[Mg(BH_4)_4]^{2-}$. On a whole, repulsive H−H effects lead, on one hand, to the elongation of the $[Mg(BH_4)_4]^{2-}$ complex anion in [001], but on the other hand, drive unit cell expansion in (001), which in turn causes a reorientation of $B1H_4$ groups and the complex anion they are coordinating to as well as its simultaneous size decrease, thus regaining body-centering. Refinement also shows that $[BH_4]^-$ is by far more mobile than K2 in terms of disordering. Interestingly, concerning the symmetry change, a similar situation has been described for the related compounds Sr_3SiO_5 and Ba_3SiO_5.[45] The difference in symmetry, space groups *Pncc* and $I4/mcm$, respectively, is attributed to the size effect of the bigger cation here, the larger Ba^{2+} interacting strongly with the complex anion $[SiO_4]^{4-}$ and thus causing its reorientation in the higher symmetric space group $I4/mcm$.

dx.doi.org/10.1021/jp212318s | J. Phys. Chem. C XXXX, XXX, XXX−XXX

Repulsive forces in the ternary borohydride as well as enhanced disorder at high temperature may also be rationalized as a simulated increase in cation size.

Thermal Expansion. The thermal behavior of both compounds $K_2M(BH_4)_4$ (M = Mg, Mn) between room temperature and 380 K is virtually identical, in both cases dominated by a pronounced positive expansion of the c-axis, a slight variation of b, and a negative expansion in a (Figure S5, Supporting Information). The coefficients of volumetric expansion are α_v = 3.19(5) and 2.17(4) × 10^{-4} K^{-1} for Mg and Mn, respectively, obtained from linear fitting in the interval 300−380 K. We would like to point out that low temperature data measured on the Mn compound as obtained from the chloride-synthesis suggest nonlinear behavior around room temperature. Up to date, no low temperature data are available for the Mg compound; this will be a topic of future investigations.

$K_3Mg(BH_4)_3$ may be described as undergoing a three-step process subject to temperature variation within the interval 295−420 K (Figure 3), as discussed above. The coefficients of volumetric and linear thermal expansion are α_v 3.24(3), α_a 1.50(4), and α_c = 0.24(4) × 10^{-4} K^{-1}, as linearly approximated in the interval 300−345 K. Roughly the same values are determined for the high temperature region T > 370 K, after having passed the anomaly (345−370 K) caused by enhanced dynamics of $[BH_4]^-$ and the symmetry change (see text above and Figure 3). Interestingly, at T < 345 K, the volume expansivity of $K_3Mg(BH_4)_5$ is identical to that of KBH_4 (Figure 3), suggesting that the KBH_4 substructure is driving the expansion throughout this first step, prior to the onset of nonlinear behavior.

Raman and Infrared Spectroscopy. The infrared and Raman spectroscopy spectra are shown in Figures 4 and 5,

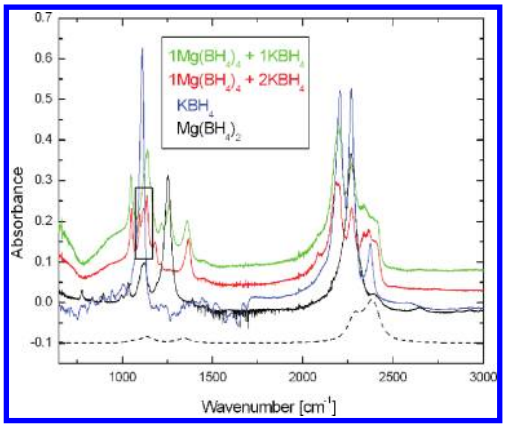

Figure 4. Infrared spectra of mixtures 1:1 and 2:1 for the Mg system. The reference spectra of the reactants are shown as well. The dashed line depicts the vibrational behavior of the calculated complex isolated anion $[Mg(BH_4)_4]^{2-}$.The black box at 1100 cm^{-1} highlights the splitting of KBH_4-like modes due to $K_3Mg(BH_4)_5$ (see text for details).

respectively. The infrared spectra of all mixtures of the Mg system show a prominent isolated single signal at about 1365 cm^{-1} (Figure 4), obviously related to $K_2Mg(BH_4)_4$ as it is present in mixture 1:1. The $Mg(BH_4)_2$-free sample B_Mg2 clearly shows that this band has no adjacent signal immediately at lower wavenumbers, which in turn points toward a dominant bidentate bonding scheme Mg···H_2B concerning $[Mg(BH_4)_2]^{2-}$, as confirmed by Rietveld refinements as well as DFT calculations. Tridentate bonding should manifest itself in

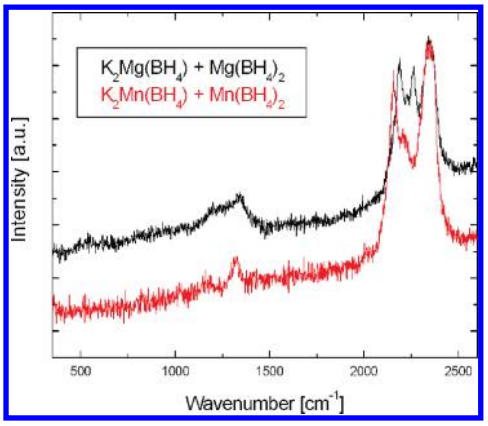

Figure 5. Raman spectra of mixtures 1:1 for both Mg and Mn systems. The legend shows the actual content of the sample after synthesis, not the composition of reactants.

additional peaks in the IR spectrum in the bending region as well as in the absence of signals around 1350 cm^{-1}, as found in the ternary Sc-compounds.[46−48] The nonbridging character of the BH_4 groups is at the origin of the splitting in stretching modes, in IR as well as Raman spectra, which is equivalent to saying that $[Mg(BH_4)_2]^{2-}$ is to a certain extent an isolated anion in both new structures probed by spectroscopy. To clarify this, the reference spectrum of the binary framework structure $Mg(BH_4)_2$ shows one stretching band only. In IR, unfortunately the signal arising from $Mg(BH_4)_2$ is quite strong, which hardly allows for an exact determination of the peaks of the new phase, spread out between 2190 and 2340 cm^{-1}, signalizing the splitting. This does agree well with the results from Raman experiments shown in Figure 5. The splitting between inner and outer B−H stretching modes increases from magnesium to manganese; possibly this reflects the different degree of isolation between the two, however likely it is due to the mass-effect only,[12] as the shift to lower wave numbers is restricted to the signals arising from stretching motion of inner BH_4 groups only (red curve in Figure 5, lower wavenumbers). The degree of splitting, for $K_2Mg(BH_4)_4$ 152 cm^{-1} and for $K_2Mn(BH_4)_4$ 182 cm^{-1}, nevertheless does reflect the isolation of $[M(BH_4)_4]^{2-}$; this becomes obvious when comparing to the even larger splitting still in the true molecular compounds $M(BH_4)_4$ with M = Zr, Hf, U.[49] The sharp intermediate peak in the Raman spectrum of the Mg compound is due to residual $Mg(BH_4)_2$; it is not observed in the Mn case, maybe due to differences in sample inhomogeneity and to the high spatial resolution of the Raman spectrometer, close to the grain size of ball-milling. This description of the structure allows for comparison with DFT calculations on complex anions $[Mn(BH_4)_4]^{2-}$ and $[Sc(BH_4)_4]^-$ and their derived spectra as reported by Severa et al.[40] and Hagemann et al.,[46] respectively. The present experimental data as well as the calculated IR spectrum of $[Mg(BH_4)_4]^{2-}$ (Figure 4) certainly compare well to the theoretical IR spectrum for the isolated molecule $[Mn(BH_4)_4]^{2-}$.[40] The infrared spectra of mixtures 1:1 and 2:1 are not straightforward to compare as both the binary borohydrides are strong absorbers and each of them occurs just in one of the mixtures. Thus, despite $K_3Mg(BH_4)_5$ being a major phase in sample B_Mg2, no immediate major difference is assessed between the spectra of both mixtures. The main visible signal in infrared, the above-mentioned bidentate fingerprint bending mode at 1365 cm^{-1}, is present in both,

dx.doi.org/10.1021/jp212318s | J. Phys. Chem. C XXXX, XXX, XXX−XXX

showing just a minor shift of 8 cm^{-1} for the mixture 2:1, the intensity remaining the same however. A closer inspection reveals that we can correlate this band with a weaker one at lower energies, that is, 1217 cm^{-1} (mixture 1:1). Sample B_Mg2 shows an intensity decrease of this latter signal, concurring with the emergence of a new band at 1183 cm^{-1}. We assign this band to $K_3Mg(BH_4)_5$. Thus, in fact two similar bending modes are visible per compound. Reconsidering this, the splitting of bending motions is 141 cm^{-1} for $K_2Mg(BH_4)_4$ and 185 cm^{-1} for $K_3Mg(BH_4)_5$. These findings, on the one hand, verify that the same complex anion must be present in both structures, with very similar geometry and environment. On the other hand, a close look at the bending motions below 1180 cm^{-1} reveals a complex splitting occurring at wavenumbers characteristic of KBH_4, present only in sample B_Mg2 (Figure 4, black box). We consider this to be a probe for the KBH_4-like substructure in $K_3Mg(BH_4)_5$. As mentioned earlier on, BH_4 groups (B2) as well as potassium atoms (K2) are disordered along the *c*-axis. On a local scale, this will lead to a spread of bond lengths K−B. This in turn will, in a bond-strength sensitive probe, show up as a split in signal in infrared spectroscopy absorptions at higher and lower wavenumbers as the consequence, corresponding to longer and shorter bond lengths in local order (see Figure 2). There is no visible evidence of this phase in the collected Raman spectra, so conclusions should not be drawn definitely.

Structural Comparison between $K_2M(BH_4)_4$ (*M* = Mg, Mn, Zn, or Cd). To systematically compare the crystal chemistry of all reported compounds of this stoichiometry, we chose to have a close look at the MK_{11} cage (Figure 6). The crystal structure can be generated starting from this building block and joining further cages in a three-dimensional array. It is thus the smallest object that contains all of the information we are interested in (it is not the asymmetric unit, however), displaying at a time the complex anion $[M(BH_4)_4]^{2-}$ as well as its nearest neighbor environment K_{11}. The extent of isolation of the anion can be judged by comparing the mean distances between the corresponding atom types.

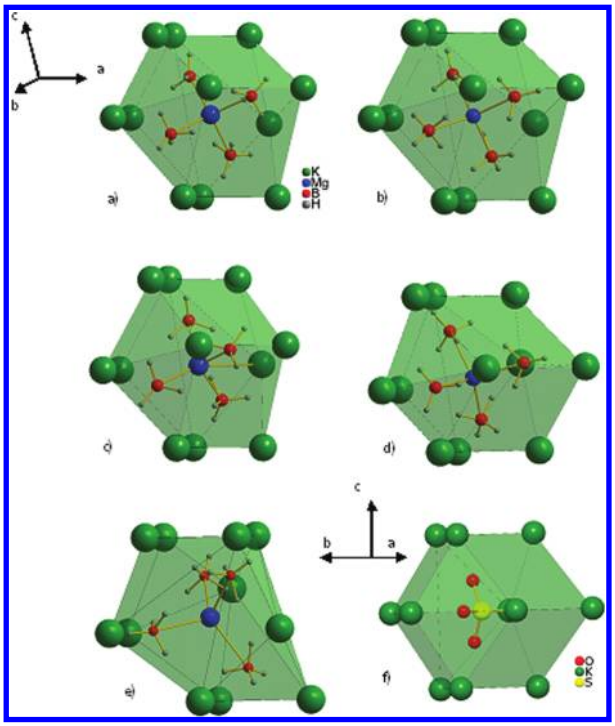

Figure 6. Comparison of the MK11 cage (Edshammar polyhedron) surrounding the complex anion in various structures of $K_2M(BH_4)_4$: (a) $K_2Mg(BH_4)_4$ from XRD, (b) $K_2Mn(BH_4)_4$, (c) $K_2Zn(BH_4)_xCl_{4-x}$,[13] (d) $K_2Mg(BH_4)_4$ from DFT, (e) $K_2Cd(BH_4)_4$,[14] and (f) K_2SO_4 (space group setting *Pbnm*). Bonds drawn between boron and central metal atoms are just for visualization; they do not represent genuine chemical bonding.

The ratio of average distances B−K/M−B from Rietveld refinement (Table 3) shows that the manganese compound is more isolated with a value of 1.41 than the magnesium analogue (1.38). In comparison, K−Zn has a value of 1.33, $KSc(BH_4)_4$ shows 1.64, and K_2SO_4 no doubt contains a truly isolated sulfate tetrahedron with 2.13. Despite the fact that the volume of the MK_{11} polyhedron (calculated with the software VESTA[50]) remains nearly unchanged within experimental errors, 262.4(9) $Å^3$ for manganese and 264.3(8) $Å^3$ for magnesium, the volume of $[M(BH_4)_4]^{2-}$ varies significantly, that is, 7.17(4) $Å^3$ for the Mn and 7.69(2) $Å^3$ for the Mg molecule, surely allowing us to conclude that there is a difference in the degree of isolation of the complex anion. Moreover, the M−H bonding scheme as well as the orientation of $[M(BH_4)_4]^{2-}$ inside the cage (see Figure 6) are virtually the same for both compounds. Mn^{2+} and Mg^{2+} have ionic radii of 80 and 71 pm, respectively, in tetrahedral coordination.[51] Given this, we observe an inverse behavior to what we would expect; not only does the Mn compound show the smaller unit cell volume (Table 1), but also on a local scale; that is, regarding the nearest neighbors surrounding *M*, the interatomic distances are shorter. We assume this to be due to electronic effects, for example, a higher degree of covalency in bonding due to the more similar electronegativities of Mn and the $[BH_4]^-$ anion. The Pauling electronegativities of Mg and Mn are 1.31 and 1.55, while that of $[BH_4]^-$ is higher than 2 according to simple group electronegativities. The average distance M−B within the complex anion is 2.503(3) and 2.454(4) for Mg and Mn, respectively (Table 3). In comparison to this, the trends reported for average M−B distances within the binary compounds are quite similar, bonds being shorter on the whole, maybe due to different extents of charge transfer from metal to $[BH_4]^-$ in binary and ternary compounds, 2.4217(9)[52] for $Mg(BH_4)_2$ and 2.4379(8) for $Mn(BH_4)_2$.[53] The framework topology of both of these compounds was claimed to be a consequence of a larger degree of directional, that is, covalent bonding, as opposed to KBH_4 or $NaBH_4$, which adopt ionic structure types, potassium and sodium being by far less electronegative.

Magnesium and manganese behave in a very similar manner in isostructural compounds. An intriguing fact found in this study is the inverse relationship of Mn and Mg concerning unit cell volume and atomic radii. Thus, considering two ionic isomorphs of these elements, the Mn-bearing compound will usually show a larger unit cell volume, which will be enhanced by polar bonding forces, usually by 1−2%. Regarding the three systems Mg, Mn, and Zn,[13] compounds have been reported among the amides as two monoclinic isomorphs (Mg, Mn) and one triclinic (Zn) of the same stoichiometry $K_2M(NH_2)_4$,[54−56] the Mn compound showing a larger unit cell volume relative to the Mg isomorph in this case. The average Mn−N distances (2.1255 Å) are larger here than the average Mg−N distances (2.0649 Å), which is contrary to our results on borohydrides. Given the fact that the compounds $K_2M(BH_4)_4$ show bidentate coordination within $[M(BH_4)_4]^{2-}$ and protic hydrogen of NH_2

dx.doi.org/10.1021/jp212318s | J. Phys. Chem. C XXXX, XXX, XXX−XXX

is pointing away from the central metal atom in the latter case (lone pairs of nitrogen coordinating to the central atom), the different trends may well be due to the nature of hydrogen in the two groups, hydridic in $[BH_4]^-$ and protic in $[NH_2]^-$.

Concerning only borohydrides again, in addition to the bond length analysis, we have calculated the volumes of both polyhedra to clarify the relation between $[M(BH_4)_4]^{2-}$ and its surrounding pentacapped trigonal prism MK_{11}. The calculated values are given in Table 3 for all systems K−Mg, Mn, Zn or Cd and for Sc for means of comparison. Both the ratios of volumes and of average bond distances decrease in the series Mn−Mg−Zn−Cd as the framework character increases, meaning that $[Mn(BH_4)_4]^{2-}$ is the most isolated anion in the series. If we consider d-metals only and consider the alkaline earth Mg as an outlier, this agrees with the order of increasing electronegativity. As the K_{11} environment approaches the complex anion, the orientation of the latter changes gradually, virtually unchanged for Mn and Mg, then rotating slightly in Zn, and finally changing orientation by 180° in Cd.

The deformation, taking the equatorial plane as a measure, shows that the pentacapped prism is most regular in the Zn compound (Figure 6), more distorted in Mg and Mn, and very distorted in Cd, being close to tetracapped in this case. Overall, the ZnK_{11} cage is flattened with respect to KMg/Mn_{11}, ratios A/h being 1.488 versus 1.25 Å, respectively (A, area of triangular face of pentacapped trigonal prism; h, height of the prism). The varying extent of deformation of KM_{11} results in modified K−B bonding. Thus, while the local environments of B2 and B3 stay essentially identical, there is an increase in boron coordination by potassium in B4, and a decrease in B1, when going from Mg to Zn, and an increase in both B3 and B4 in Cd. On the other hand, as stated in ref 13, the compound $K_2Zn(BH_4)_4$ investigated was a chemically disordered chloride/borohydride, as the highest degree of substitution by chloride was refined on the B1 and B4 sites, and the different deformation may just be due to chemical substitution. Currently, efforts to achieve a pure ternary K−Zn compound are underway. They will help in determining the role that electronic effects may be playing for distortion as well as framework building.

Decomposition Analysis by in Situ SR-PXD. The decomposition pathways of mixtures 1:1 as synthesized from pure borohydrides are very similar. In the system K−Mg−BH_4 (sample B_Mg1), $K_2Mg(BH_4)_4$ and the binary compound $Mg(BH_4)_2$ seem to behave as an eutectic mixture with relative molar compositions at the eutectic minimum, the eutectic temperature being 416 K, as verified by an endothermic event in DTA analysis (Figure 7) corresponding to melting. Decomposition of $Mg(BH_4)_2$ has been reported to occur at 518 K[57] or 546 K.[58] A eutectic melting has been observed for the system $Mg(BH_4)_2$−$LiBH_4$ as well.[59,60] As for the K−Mn system (sample B_Mn1), it is supposedly also dominated by a melting mechanism, however not eutectic, but with a temperature gap between the melting of $Mn(BH_4)_2$ (389 K as opposed to reported 450 K in chloride-containing mixtures[53]) and that of $K_2Mn(BH_4)_4$ (420 K). Furthermore, in the K−Mn system, the decomposition of $K_2Mn(BH_4)_4$ is observed to generate KBH_4 and a further new phase, which we have identified as $KMn(BH_4)_3$ and which is derived from the perovskite structure. With the present data, it was impossible to accurately solve the crystal structure, although the average structure is given in the Supporting Information (Figure S6), as well as the temperature ramp for sample B_Mn1 (Figure S7).

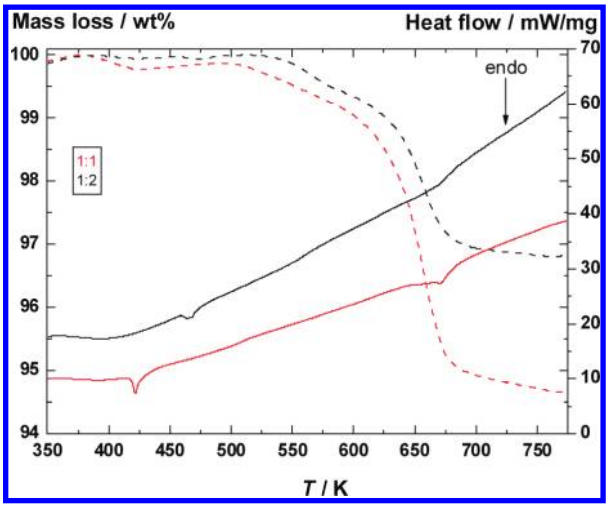

Figure 7. TGA and DTA curves for mixtures 1:1 (red) and 2:1 (black) of the Mg system. TGA, dashed; DTA, solid.

We are currently investing efforts into maximizing the yield to solve this problem. The phase was indexed from sample B_Mn1 at 458 K on the basis of 12 Bragg peaks in a tetragonal cell with lattice constants a = 7.066 and c = 10.065 Å. Systematic extinctions strongly suggest space group $P4_2/mbc$ being a nonisomorphic subgroup of $P4/mbm$, which corresponds to the symmetry of the prototype $NaNbO_3$, with halved c-axis.[61] However, many space groups and supercells were tested, none of which allowed for satisfactory refinements, R not going below 25%. Attempts to model in direct space favor a high degree of disorder, and thus a low symmetry of the smaller cells. We believe that this is a strong indication of missed reflections of a superstructure we are not able to visualize with X-ray diffraction. A similar situation has occurred in the case of $Y(BH_4)_3$. Initially, the high temperature phase was solved in Pm-3 m from XRD,[62] which was later on corrected to Fm-3c in a 2 × 2 × 2 supercell, with the help of neutron data.[63] We have modeled $KMn(BH_4)_3$ in $I4/mcm$ (structure type $SrZrO_3$[64]), which is a supergroup to $P4/mbm$ and a nonisomorphic subgroup to Fm-3c. Comparing both the HT-phase of $Y(BH_4)_3$ and $KMn(BH_4)_3$, one may describe the latter as a filled variant of the former. A HT-$Y(BH_4)_3$ framework of ReO_3 type will not be charge balanced if Y^{3+} is substituted by Mn^{2+}. Balancing is thus achieved by filling the voids between $Mn(BH_4)_6$ octahedra with potassium atoms in 12-fold cuboctahedral coordination, thus generating a perovskite type structure. All trials resulted in an atomic arrangement most certainly related to a perovskite. This is very interesting as no perovskite-derived borohydride has been observed yet up to date. The fact that Mn^{2+} is octahedrally coordinated by $[BH_4]^-$ here leaves a lot of space for planned investigations in the future. This new phase in turn shows its own decomposition pathway to most likely one of the intermediate phases containing higher boranes, possibly $B_{12}H_{12}$ as we assume, as its diffraction resembles that of recently reported $CaB_{12}H_{12}$.[65]

The main difference with respect to mixtures 2:1 is of course the behavior of $K_3Mg(BH_4)_5$, which is only formed in the K−Mg system (sample B_Mg2) and whose thermal evolution has been described above. In this mixture, the initial main phase $K_3Mg(BH_4)_5$ starts to decompose in a first major event, ranging from approximately 353 to 385 K, via segregation to $K_2Mg(BH_4)_4$ and KBH_4 (Figure S8). In this temperature interval, we can clearly see the weak reflections disappearing,

dx.doi.org/10.1021/jp212318s | J. Phys. Chem. C XXXX, XXX, XXX−XXX

which forced us to index $K_3Mg(BH_4)_5$ in a *P*-lattice (Supporting Information Figure S9). However, the stability of the phase is not exceeded until about 433 K, where we can see the remnant intensity of its strong signals disappearing; additionally, this is manifested in a slight increase of the amount of KBH_4, indicating a final minor decomposition event. The temperature stability of $K_2Mg(BH_4)_4$ is enhanced in the mixture 2:1. While its melting is observed at 416 K in composition 1:1, it remains crystalline up to 468 K in 2:1, as confirmed by thermal analysis. The higher melting point may be due to the phase being stabilized by $K_3Mg(BH_4)_5$, which in turn acts as a generator of $K_2Mg(BH_4)_4$. The endothermic event at 468 K is divided into two steps with a difference of 4 K; this could be due to the additional final disappearing of remnant $K_3Mg(BH_4)_4$, which cannot be resolved by powder diffraction any longer.

As $K_3M(BH_4)_5$ does not form in the K−Mn system (at the applied conditions), the temperature-dependent evolution of mixture 2:1 is essentially the same as for 1:1 as well as the decomposition temperature of $K_2Mn(BH_4)_4$, 421 versus 420 K in mixtures 2:1 and 1:1, respectively. The new phase $KMn(BH_4)_3$ forms also in mixture 2:1, although with a lower yield, verifying the assumed stoichiometry, which should result in a higher yield in systems with a greater manganese content. Both temperatures are confirmed by DTA.

A point that calls for attention is the fact that the decomposition of $K_3Mg(BH_4)_5$ does not show up as a distinct signal in thermal analysis. The conversion of $K_3Mg(BH_4)_5$ to $K_2Mg(BH_4)_4$ and KBH_4 is a continuous process as evidenced by sequential refinements of T-ramps. The negative slope of the DTA curve at lower temperatures does not reflect this process; it is actually an instrument artifact. We assume that the absence of a signal in thermodynamic tracking may be due to very similar standard enthalpies of formation of the involved compounds. In fact, both products from the decomposition are to some extent "ready-made" in $K_3Mg(BH_4)_5$ as discussed above. So, as stated earlier on, the process of decomposition may be described more accurately as the disproportionation of an adduct, with just a slight energy drop on the products side. The low temperature would strongly favor this idea.

Thermal Analysis. The results from simultaneous thermogravimetric (TGA) and differential thermal analysis (DTA) measured for the mixtures KBH_4−$Mg(BH_4)_2$ 1:1 and 2:1 are displayed in Figure 7. The bump at low temperatures and the slope, observed in the DTA data, as well as the continuous increase in the TGA data are instrumental artifacts due to buoyancy.

The first endothermic peak observed for mixture 1:1 occurs at 423 K and corresponds to the decomposition of $K_2Mg(BH_4)_4$. The endothermic peak is associated with a mass loss of 0.5 wt % from 378 to 423 K. A mass loss of 1.2 wt % is also observed between 503 and 633 K. However, no thermodynamic event is observed in this region. The mass loss may originate from an unknown compound or from residual amorphous $Mg(BH_4)_2$. Another endothermic peak is observed at 668 K, which appears to consist of two peaks, a broad and a sharper peak. From 633 to 703 K a mass loss of 3.3 wt % is observed, which may arise from the decomposition of an unknown intermediate possibly associated with the endothermic peak, but may also be the due to the decomposition of MgH_2. Above 703 K, the decomposition of remaining KBH_4 is initiated, which accounts for the observed mass loss from 703 to 773 K. The total mass loss for the mixture KBH_4−$Mg(BH_4)_2$ 1:1 is 5.5 wt % from room temperature to 773 K, and the calculated mass loss for this sample is 11.2 wt %.

Two endothermic peaks are observed for the mixture KBH_4−$Mg(BH_4)_2$ 2:1 at 464 and 468 K, respectively, which correspond to the decomposition of $K_2Mg(BH_4)_4$ and $K_3Mg(BH_4)_5$, as discussed earlier. The first mass loss of 1 wt % occurs from 503 to 633 K. Again, no thermodynamic peak is observed in the region, as for the 1:1 mixture. From 633 to 703 K, the same temperature range as for the mixture KBH_4−$Mg(BH_4)_2$ 1:1, the largest mass loss for mixture 2:1 is initiated, which amounts to 1.9 wt %. This is also associated with a weak and broad endothermic peak at 668 K. Both mass losses observed for the mixture 2:1 probably correspond to the similar decompositions as discussed for mixture 1:1. Decomposition of remaining KBH_4 occurs at $T > 703$ K. The total mass loss for the mixture 2:1 sample amounts to 3.2 wt %, and the calculated mass loss for this sample is 9.9 wt % based on the hydrogen content.

CONCLUSIONS

This study describes the detailed analysis of the systems $M(BH_4)_2$−KBH_4 (M = Mg or Mn). Structural comparisons on the herein discovered isomorphs $K_2M(BH_4)_4$ extend the analogies found in frameworks of the binary $M(BH_4)_2$ to the ternary containing the complex anion $[M(BH_4)_4]^{2-}$. Contrary to expectation, the Mn compound shows a smaller unit cell volume. Both virtually identical structures reveal different degrees of isolation of the complex anion. Periodic DFT calculations on $K_2Mg(BH_4)_4$ as well as those on the isolated molecule $[M(BH_4)_4]^{2-}$ reveal a predominantly bidentate M···H_2B bonding scheme and verify the crystal structure as solved ab initio from synchrotron powder diffraction data. $K_2M(BH_4)_4$ crystallizes as a distorted K_2SO_4-type structure in space group $P2_1/n$. Decomposition temperatures of both isomorphs are within uncertainties; however, a composition-dependent stabilization of the phase is found in the Mg system, as well as a eutectic behavior. Furthermore, the study highlights the complexity of phase equilibria as stated by the different decomposition temperatures, but also by the finding of two further hitherto unreported phases, $K_3Mg(BH_4)_5$ and $KMn(BH_4)_3$. The former crystallizes in space group $P4_2/mbc$ and is described as an intergrowth of KBH_4 and $K_2Mg(BH_4)_4$, derived from the Cs_3CoCl_5-type ($I4/mcm$), and is discussed in terms of positional disorder believed to be at the origin of its low decomposition temperature as well as in terms of a sluggish phase transition possibly regaining body centering lost originally due to $[BH_4]^-$ orientation. The latter, $KMn(BH_4)_3$, is not solved unambiguously but is nevertheless shown to crystallize in a tetragonal perovskite-type derived from the $NaNbO_3$-type ($P4/mbm$), being the first borohydride reported to crystallize in a true perovskite structure, meaning that the transition metal is octahedrally coordinated by BH_4 groups. The individual conditions under which both phases form, both occurring only in one of the systems, corroborate the high sensitivity of the phase stabilities of borohydrides with respect to synthesis conditions.

The findings of this study emphasize once more the tendency of ternary borohydrides to adopt structures closely related to iono-covalent structure types known from oxides and halides. This should be an important hint for the ongoing search of new $[BH_4]^-$-based compounds with tailored properties, going further than hydrogen storage.

dx.doi.org/10.1021/jp212318s | J. Phys. Chem. C XXXX, XXX, XXX−XXX

■ ASSOCIATED CONTENT

Supporting Information

Rietveld refinement plots, T-ramps, temperature-dependent evolution of lattice parameters, average structural model of $KMn(BH_4)_3$ as graphics, and crystal data from refined and calculated models as CIF files. This material is available free of charge via the Internet at http://pubs.acs.org.

■ AUTHOR INFORMATION

Corresponding Author

*Tel.: +41 2237 96079 (P.S.), +41 2237 96450 (R.C.). Fax: +41 2237 96108 (P.S.), +41 2237 96108 (R.C.). E-mail: pascal.schouwink@unige.ch (P.S.), radovan.cerny@unige.ch (R.C.).

Notes

The authors declare no competing financial interest.

■ ACKNOWLEDGMENTS

T.R.J., B.R., and M.B.L. thank the Danish Research Council for Nature and Universe (Danscatt), the Danish National Research Foundation (Centre for Materials Crystallography), the Danish Strategic Research Council (Centre for Energy Materials), and the Carlsberg Foundation for funding. P.S. and R.C. thank NCCR MaNEP and the Swiss National Science Foundation for funding. We acknowledge SNBL for the beamtime allocation and providing in-house beamtime. V.D'A., H.H. and L.D.L.M. also acknowledge supercomputer time at the Swiss National Supercomputing Centre (CSCS) under project ID s103, and at the Center for Advanced Modeling Science (CADMOS) under project ID CTESIM. The financial support for CADMOS and for the Blue Gene/P system is provided by Geneva Canton, Vaud Canton, fondation of Hans Wilsdorf, fondation of Louis-Jeantet, the University of Geneva, the University of Lausanne, and the Ecole Polytechnique Fédérale de Lausanne.

■ REFERENCES

(1) Orimo, S.; Nakamori, Y.; Eliseo, J. R.; Züttel, A.; Jensen, C. M. *Chem. Rev.* **2007**, *107*, 4111−4132.
(2) Ravnsbæk, D. B.; Filinchuk, Y.; Černý, R.; Jensen, T. R. *Z. Kristallogr.* **2010**, *225*, 557−569.
(3) Rude, L. H.; Nielsen, T. K.; Ravnsbæk, D. B.; Bösenberg, U.; Ley, M. B.; Richter, B.; Arnbjerg, L. M.; Dornheim, M.; Filinchuk, Y.; Besenbacher, F.; Jensen, T. R. *Phys. Status Solidi A* **2011**, *208*, 1754−1773.
(4) Nakamori, Y.; Miwa, K.; Ninomiya, A.; Li, H.; Ohba, N.; Towata, S.; Züttel, A.; Orimo, S. *Phys. Rev. B* **2006**, *74*, 045126.
(5) Schrauzer, G. N. *Naturwissenschaften* **1995**, *42*, 438.
(6) Nielsen, T. K.; Besenbacher, F.; Jensen, T. R. *Nanoscale* **2011**, *3*, 2086−2098.
(7) Nielsen, T. K.; Bösenberg, U.; Gosalawit, R.; Dornheim, M.; Cerenius, Y.; Besenbacher, F.; Jensen, T. R. *ACS Nano* **2010**, *4*, 3903−3908.
(8) Li, H.-W.; Yan, Y.; Orimo, S.-I.; Züttel, A.; Jensen, C. M. *Energies* **2011**, *4*, 185−214.
(9) Mosegard, L.; Møller, B.; Jørgensen, J.; Filinchuk, Y.; Cerenius, Y.; Hanson, J. C.; Dimasi, E.; Besenbacher, F.; Jensen, T. R. *J. Phys. Chem. C* **2008**, *112*, 1299−1303.
(10) Arnbjerg, L. M.; Ravnsbæk, D. B.; Filinchuk, Y.; Vang, R. T.; Cerenius, Y.; Besenbacher, F.; Joergensen, J.-E.; Jakobsen, H. J.; Jensen, T. R. *Chem. Mater.* **2009**, *21*, 5772−5782.
(11) Matsuo, M.; Orimo, S.-I. *Adv. Energy Mater.* **2011**, *1*, 162−171.
(12) Černý, R.; Penin, N.; D'Anna, V.; Hagemann, H.; Durand, E.; Ruzicka, J. *Acta Mater.* **2011**, *59*, 5171−5180.
(13) Černý, R.; Ravnsbæk, D. B.; Schouwink, P.; Filinchuk, Y.; Penin, N.; Teyssier, J.; Smrčok, L.; Jensen, T. R. *J. Phys. Chem. C* **2012**, *116*, 1563−1571.
(14) Ravnsbæk, D. B.; Sørensen, L. H.; Filinchuk, Y.; Besenbacher, F.; Jensen, T. R. *Angew. Chem., Int. Ed.*, *51*, 3582−3586.
(15) Hohenberg, P.; Kohn, W. *Phys. Rev.* **1964**, *136*, B864.
(16) Kohn, W.; Sham, L. J. *Phys. Rev.* **1965**, *140*, A1133.
(17) Hagemann, H.; Černý, R. *Dalton Trans.* **2010**, *39*, 6006−6012.
(18) Hammersley, A. P.; Svensson, S. O.; Hanfland, M.; Fitch, A. N.; Häusermann, D. *High Pressure Res.* **1996**, *14*, 235−248.
(19) Vogel, S.; Ehm, L.; Knorr, K.; Braun, G. *Adv. X-Ray Anal.* **2002**, *45*, 31−33.
(20) Favre-Nicolin, V.; Černý, R. *J. Appl. Crystallogr.* **2002**, *35*, 734−743.
(21) Seifert, H. J.; Uebach, J. *J. Solid State Chem.* **1985**, *59*, 86−94.
(22) Horowitz, A.; Amit, M.; Makovsky, J. *J. Solid State Chem.* **1982**, *43*, 107−125.
(23) Arnold, H.; Kurtz, W.; Richter Zinnius, A.; Bethke, J.; Heger, G. *Acta Crystallogr., Sect. B* **1981**, *37*, 1643−1651.
(24) Coelho, A. A. TOPAS-Academic; http://members.optusnet.com.au/~alancoelho.
(25) Spek, A. L. *PLATON*; University of Utrecht: The Netherlands, 2006.
(26) Powell, H. M.; Wells, A. F. *J. Chem. Soc.* **1935**, 359−362.
(27) Perdew, J. P.; Burke, K.; Ernzerhof, M. *Phys. Rev. Lett.* **1996**, *77*, 3865−3868.
(28) Gonze, X; Amadon, B.; Anglade, P.-M.; Beuken, J.-M.; Bottin, F.; Boulanger, P.; Bruneval, F.; Caliste, D.; Caracas, R.; Côté.; et al. *Comput. Phys. Commun.* **2009**, *180*, 2582−2615 and references therein..
(29) Troullier, N.; Martins, J. L. *Phys. Rev. B* **1991**, *43*, 1993−2006.
(30) Kleinman, L.; Bylander, D. M. *Phys. Rev. Lett.* **1982**, *48*, 1425−1428.
(31) Monkhorst, H. J.; Pack, J. D. *Phys. Rev. B* **1976**, *13*, 5188−5192.
(32) Slater, J. C. *Phys. Rev.* **1951**, *81*, 385−390.
(33) Vosko, S. H.; Wilk, L.; Nusair, M. *Can. J. Phys.* **1980**, *58*, 1200−1211.
(34) Becke, A. D. *Phys. Rev. A* **1988**, *38*, 3098−3100.
(35) Lee, C.; Yang, W.; Parr, R. G. *Phys. Rev. B* **1988**, *37*, 785−789.
(36) Becke, A. D. *J. Chem. Phys.* **1993**, *98*, 5648−5652.
(37) Schäfer, A.; Huber, C.; Ahlrichs, R. *J. Chem. Phys.* **1994**, *100*, 5829−5835.
(38) Ahlrichs, R.; Bär, M.; Häser, M.; Horn, H.; Kälmel, C. *Chem. Phys. Lett.* **1989**, *162*, 165−169.
(39) Nickels, E. A.; Jones, M. O.; David, W. I. F.; Johnson, S. R.; Lowton, R. L.; Sommariva, M.; Edwards, P. P. *Angew. Chem., Int. Ed.* **2008**, *47*, 2817−2819.
(40) Severa, G.; Hagemann, H.; Longhini, M.; Kaminski, J. W.; Weselowski, T. A.; Jensen, C. M. *J. Phys. Chem. C* **2010**, *114*, 15516−15521.
(41) Černý, R.; Ravnsbæk, D. B.; Severa, G.; Filinchuk, Y.; D'Anna, V.; Hagemann, H.; Skibsted, J.; Jensen, C. M.; Jensen, T. R. *J. Phys. Chem. C* **2010**, *114*, 19540−19549.
(42) Shevlin, S. A.; Guo, Z. X. *Chem. Soc. Rev.* **2009**, *38*, 211−225.
(43) Renaudin, G.; Gomes, S.; Hagemann, H.; Keller, L.; Yvon, K. *J. Alloys Compd.* **2004**, *375*, 98−106.
(44) Rao, B. K.; Jena, P. *Phys. Rev. B* **1985**, *31*, 6726−6730.
(45) Tillmanns, E.; Grosse, H.-P. *Acta Crystallogr.* **1978**, *B34*, 649−651.
(46) Hagemann, H.; Longhini, M.; Kaminski, J. W.; Wesolowski, T. A.; Černý, R.; Penin, N.; Sorby, M. H.; Hauback, B. C.; Severa, G.; Jensen, C. M. *J. Phys. Chem. A* **2008**, *112*, 7551−7555.
(47) Černý, R.; Severa, G.; Ravnsbæk, D.; Filinchuk, Y.; D'Anna, V.; Hagemann, H.; Haase, D.; Jensen, C. M.; Jensen, T. R. *J. Phys. Chem. C* **2010**, *114*, 1357−1364.
(48) Černý, R.; Ravnsbæk, D.; Severa, G.; Filinchuk, Y.; D'Anna, V.; Hagemann, H.; Haase, D.; Skibsted, J.; Jensen, C. M.; Jensen, T. R. *J. Phys. Chem. C* **2010**, *114*, 19540−19549.
(49) Marks, T. J.; Kolb, J. R. *Chem. Rev.* **1977**, *77*, 263−293.
(50) Momma, K.; Izumi, F. *J. Appl. Crystallogr.* **2011**, *44*, 1272−1276.
(51) Shannon, R. D. *Acta Crystallogr.* **1976**, *A32*, 751−767.

(52) Filinchuk, Y.; Chernyshov, D.; Dmitriev, V. *Z. Kristallogr.* **2008**, *223*, 649−659.
(53) Černý, R.; Penin, N.; Hagemann, H.; Filinchuk, Y. *J. Phys. Chem. C* **2009**, *113*, 9003−9007.
(54) Jacobs, H.; Birkenbeul, J.; Kockelkorn, J. *J. Less-Common Met.* **1984**, *97*, 205−214.
(55) Drew., M. *Rev. Chim. Miner.* **1975**, *12*, 419−426.
(56) Fröhling, B.; Jacobs, H. *Z. Anorg. Allg. Chem.* **1997**, *623*, 1103−1107.
(57) Riktor, M. D.; Sørby, M. H.; Chłopek, K; Fichtner, M.; Buchter, F.; Züttel, A.; Hauback, B. C. *J. Mater. Chem.* **2007**, *17*, 4939−4942.
(58) Soloveichik, G. L.; Gao, Y.; Rijssenbeek, J.; Andrus, M.; Kniajanski, S.; Bowman, R. C., Jr.; Hwang, S.-J.; Zhao, J.-C. *Int. J. Hydrogen Energy* **2009**, *34*, 916−928.
(59) Bardají, E. G.; Zhao-Karger, Z.; Boucharat, N.; Nale, A.; Van Stetten, M. J.; Lohstroh, W.; Röhm, E.; Catti, M.; Fichtner, M. *J. Phys. Chem. C* **2011**, *115*, 6095−6101.
(60) Hagemann, H.; D'Anna, V.; Rapin, J.-P.; Černý, R.; Filinchuk, Y.; Kim, K. C.; Scholl, D. S.; Parker, S. F. *J. Alloys Compd.* **2011**, S688−S690.
(61) Glazer, A. M.; Megaw, H. D. *Acta Crystallogr., Sect. A* **1973**, *29*, 489−495.
(62) Ravnsbæk, D. B.; Filinchuk, Y.; Černý, R.; Ley, M. B.; Haase, D.; Jakobsen, H. J.; Skibsted, J.; Jensen, T. R. *Inorg. Chem.* **2010**, *49*, 3801−3809.
(63) Frommen, C.; Aliouane, N.; Deledda, S.; Fonneløp, J. E.; Grove, H.; Lieutnant, K.; Llamas-Jansa, I.; Sartori, S.; Sørby, M. H.; Hauback, B. C. *J. Alloys Compd.* **2010**, *496*, 710−716.
(64) Ahtee, M.; Glazer, A. M.; Hewat, A. W. *Acta Crystallogr., Sect. B* **1978**, *34*, 752−758.
(65) Stavila, V.; Her, J.-H.; Zhou, W.; Hwang, S.-J.; Kim, C.; Ottley, L. A. M.; Udovic, T. J. *J. Solid State Chem.* **2010**, *183*, 1133−1140.